Title

The structure of Mycobacterium thermoresistibile MmpS5 reveals a conserved disulfide bond across mycobacteria.

Journal

Metallomics, 16(3)

Authors

Cuthbert, Bonnie

Mendoza, Jessica

de Miranda, Rodger

et al.

Publication Date

2024-03-12

DOI

10.1093/mtomcs/mfae011

Peer reviewed

Metallomics, 16, 2024, mfae011
https://doi.org/10.1093/mtomcs/mfae011
Advance access publication date: 29 February 2024
Communication

The structure of *Mycobacterium thermoresistibile* MmpS5 reveals a conserved disulfide bond across mycobacteria

Bonnie J. Cuthbert[1], Jessica Mendoza[1], Rodger de Miranda[1], Kadamba Papavinasasundaram[2], Christopher M. Sassetti[2] and Celia W. Goulding [1,3,*]

[1]Department of Molecular Biology & Biochemistry, University of California Irvine, Irvine, CA 92697, USA, [2]Department of Microbiology and Physiological Systems, UMass Chan Medical School, Worcester, MA 01605, USA and [3]Department of Pharmaceutical Sciences, University of California, Irvine, Irvine, CA 92697, USA
*Correspondence: University of California, Irvine, 2212 Natural Sciences 1, Mail Code: 3900, Irvine, CA 92697, USA. E-mail: celia.goulding@uci.edu

Abstract

The tuberculosis (TB) emergency has been a pressing health threat for decades. With the emergence of drug-resistant TB and complications from the COVID-19 pandemic, the TB health crisis is more serious than ever. *Mycobacterium tuberculosis* (Mtb), the causative agent of TB, requires iron for its survival. Thus, Mtb has evolved several mechanisms to acquire iron from the host. Mtb produces two siderophores, mycobactin and carboxymycobactin, which scavenge for host iron. Mtb siderophore-dependent iron acquisition requires the export of apo-siderophores from the cytosol to the host environment and import of iron-bound siderophores. The export of Mtb apo-siderophores across the inner membrane is facilitated by two mycobacterial inner membrane proteins with their cognate periplasmic accessory proteins, designated MmpL4/MmpS4 and MmpL5/MmpS5. Notably, the Mtb MmpL4/MmpS4 and MmpL5/MmpS5 complexes have also been implicated in the efflux of anti-TB drugs. Herein, we solved the crystal structure of *M. thermoresistibile* MmpS5. The MmpS5 structure reveals a previously uncharacterized, biologically relevant disulfide bond that appears to be conserved across the *Mycobacterium* MmpS4/S5 homologs, and comparison with structural homologs suggests that MmpS5 may be dimeric.

Keywords: *Mycobacterium tuberculosis*, MmpS4, MmpS5, iron acquisition

Graphical abstract

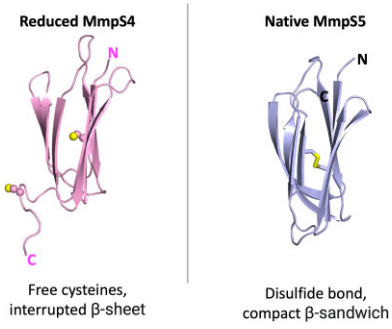

While an NMR structure for a reduced MmpS4 was previously solved, the crystal structure for a non-reduced MmpS5 reveals a disulfide bond that appears to be conserved across *Mycobacterium* MmpS4/S5 homologs.

Introduction

Tuberculosis (TB), caused by the pathogen *Mycobacterium tuberculosis* (Mtb), has been classified as a critical health crisis for decades. The World Health Organization defined TB as a global emergency in 1993. In 2024, TB still remains a looming presence with 10 million cases per year.[1] Indeed, TB-related deaths increased with the COVID-19 pandemic, culminating in 1.6 million deaths in 2021, and TB will soon become the leading cause of death worldwide from a single infectious agent. While the TB emergency was exacerbated by the COVID-19 pandemic, the emergence of multidrug-resistant and extensively drug-resistant TB has long been a pressing concern.[2] Current TB treatments require an extensive drug regimen, and patient noncompliance due to treatment length, accessibility, and side effects contributes to emerging drug-resistant strains.[2] With widespread and mounting TB cases, drug resistance, and difficulties in TB treatment, there is a critical need for new TB therapeutics and therapeutic targets.[3,4]

To survive, Mtb must sequester iron from its human host. To facilitate the acquisition of host iron, Mtb has both siderophore-mediated and heme-iron uptake pathways, of which the siderophore-mediated uptake pathway is more effective.[5–7] Mtb produces two iron-specific siderophores, hydrophobic mycobactin and hydrophilic carboxymycobactin. The efflux of Mtb siderophores through the inner membrane is mediated by inner membrane efflux pumps and their periplasmic accessory proteins, MmpL4/MmpS4 (MmpL4/S4) and MmpL5/MmpS5 (MmpL5/S5),[8] whereby MmpL is mycobacterial membrane protein large and MmpS is mycobacterial membrane protein small.[9]

Received: October 31, 2023. **Accepted:** February 10, 2024

MmpL proteins are members of the resistance nodulation division (RND) superfamily of efflux pumps.[9] Mtb has 12 functional MmpLs, which have been implicated in the transport of various substrates across the inner membrane, such as Mtb lipids, carbohydrates, and siderophores.[10,11] MmpLs are often located near genes associated with lipid metabolism and polyketide biosynthesis.[12] Like other RND proteins, MmpLs are powered by proton motive force and composed of 12 transmembrane helices, with both N- and C-terminal periplasmic domains and porter subdomains, and some have an additional middle docking subdomain.[5,13,14] Like RND proteins, several MmpL proteins, including MmpL4 and MmpL5, have associated periplasmic adaptor MmpS proteins. It remains to be seen whether MmpL proteins are homotrimeric efflux pumps as observed for RND proteins.[15] MmpL3, for example, appears to be a monomer[14,16,17]; however, recent work suggests that Mtb MmpL5 forms homotrimers, but only in the presence of MmpS5, indicating a potential role for MmpS proteins in MmpL oligomerization.[18]

MmpL4/S4 and MmpL5/S5 complexes have been implicated in siderophore export. First, the Mtb Δ*mmpS4/mmpS5* (Mtb Δ*mmpS4/S5*) mutant and the Mtb Δ*mmpL4/mmpL5* mutant do not grow under low-iron conditions, and this attenuation is not rescued by media supplemented with ferric carboxymycobactin.[8,19] Second, the Mtb Δ*mmpS4/S5* mutant produces less cell-associated and secreted siderophores compared to wild-type Mtb, and siderophore biosynthesis is unaffected, so MmpS4 and MmpS5 appear to be involved in siderophore export.[8] Third, Mtb Δ*mmpS4/S5* was shown to accumulate carboxymycobactin, unlike the wild-type or the complemented mutant, indicating that MmpS4 and MmpS5 are required for carboxymycobactin export.[6] Notably, *in vivo* complementation experiments show that MmpL4 requires MmpS4 for wild-type growth, while MmpL5 can form a stable efflux pump with either MmpS4 or MmpS5,[8] indicating that MmpL5 is more promiscuous in its accessory protein requirement. Interestingly, it has been shown that MmpL4/S4 and MmpL5/S5 complexes are involved in siderophore recycling, and if interrupted, the buildup of excess cytosolic siderophores results in attenuated growth, suggesting that Mtb siderophores are toxic in high concentrations.[6,19]

As iron acquisition is essential to Mtb, it is hardly surprising that MmpL4/S4 and MmpL5/S5 complexes are necessary for Mtb virulence in mice infections. Indeed, both MmpL4 and MmpL5 are required for Mtb virulence in mice infections.[9,20] While the Mtb Δ*mmpS4/S5* mutant results in a loss of virulence in mice, single mutant variants Δ*mmpS4* or Δ*mmpS5* show no phenotype.[8] Strikingly, Δ*mmpS4/S5* had 10 000 times lower bacterial burden in mouse lungs and was no longer fatal to mice.

Notably, MmpL4/S4 and MmpL5/S5 have been associated with drug resistance and are believed to act as a multidrug efflux pump. Several studies in mycobacteria—Mtb, *M. abscessus*, and *M. avium intracellulare*—have shown that the upregulation and overexpression of *mmpL5/S5* result in resistance to several drugs such as thioacetazone, bedaquiline, and clofazimine.[21–28] Recently, MmpL4/S4 was also shown to form a drug efflux pump in Mtb, where Δ*mmpL4/S4* and Δ*mmpL5/S5* resulted in increased susceptibility to bedaquiline, clofazimine, rifabutin, and econazole.[29] Interestingly, MmpL5/S5 is a more efficient drug efflux pump for detoxification of bedaquiline than MmpL4/S4.[29]

In summary, the MmpL4/S4 and MmpL5/S5 inner membrane complexes are involved in the export of Mtb siderophores essential for iron acquisition and also prevent accumulation of toxic siderophores. Furthermore, MmpL4/S4 and MmpL5/S5 have been implicated in the efflux of multiple anti-TB drugs. As MmpL4/S4 and MmpL5/S5 play such critical roles in Mtb, these complexes are attractive anti-TB drug targets. To elucidate their mechanism of action and to provide a template for structure-based drug design, it is important to determine their atomic resolution structures.

Previously, the structure of one of the periplasmic accessory proteins, Mtb MmpS4, was determined by nuclear magnetic resonance (NMR).[8] Here, using X-ray crystallography, we have characterized MmpS5 from the closely related Mtb homolog, *M. thermoresistibile* (Mth). The structure of Mth MmpS5 revealed a disulfide bond that was absent in the NMR structure. Notably, the disulfide-bond-forming cysteine residues are conserved across MmpS4/S5 homologs from various mycobacterial organisms. Further, mass spectrometry (MS) experiments with purified Mth MmpS5, and *M. smegmatis* (Msm) MmpS4/S5 homologs expressed *in vivo*, indicate that the disulfide bond is present under native conditions in mycobacteria, suggesting that it is physiologically relevant. Lastly, the crystallographic asymmetric unit revealed a convincing Mth MmpS5 dimer. Size exclusion chromatography experiments confirmed that both Mth and Mtb MmpS5 are dimeric in solution, which is a striking difference from the monomeric Mtb MmpS4 NMR structure.[8]

Methods

Expression and purification of Mtb and Mth MmpS5

The DNA sequence for Mtb *mmpS5* encoding residues 46-142 or Mth *mmpS5* encoding residues 46-143 was optimized for expression in *Escherichia coli* and cloned into pGEX-6P using *BamHI* and *XhoI* restriction sites (GenScript). BL21 (DE3) Gold *E. coli* cells were transformed with the resulting plasmid, which were then grown in Luria broth (LB) with 100 µg/ml ampicillin overnight and used to inoculate ampicillin-supplemented LB at 37°C. When the cells reached an optical density at a wavelength of 600 nm of 0.6, the temperature was reduced to 18°C, induced with 0.5 mM isopropyl β-D-1-thiogalactopyranoside, and grown for a further 18 h before harvesting at 5000 r.p.m. for 15 min. The cell pellet was resuspended in 0.1 M phosphate buffer, 0.5 M NaCl, pH 7.4, with 0.1 mM phenylmethylsulfonyl fluoride and lysozyme and 1 mM β-mercaptoethanol, lysed by sonication, and centrifuged at 14 000 r.p.m. to remove cell debris. The resulting supernatant was sterile filtered (Sartorious Minisart GF) and applied to a glutathione S-transferase (GST) HiTrap 5 ml column (5 ml, GE Healthcare). The GST column was washed with phosphate-buffered saline (140 mM NaCl, 2.7 mM KCl, 10 mM Na_2HPO_4, and 1.8 mM KH_2PO_4, pH 7.4) supplemented with 1 mM dithiothreitol (DTT), and Mth MmpS5-GST was eluted from the column in 50 mM Tris, pH 8, 200 mM NaCl, 10 mM reduced glutathione, and 1 mM DTT. Fractions containing Mtb or Mth MmpS5-GST were identified by sodium dodecyl sulfate-polyacrylamide gel electrophoresis, pooled, and dialyzed against 50 mM Tris, pH 7.4, 150 mM NaCl, and 1 mM DTT in the presence of PreScission Protease (Cytiva) to remove the GST tag. Following dialysis and GST cleavage, the protein was concentrated before further purification by a Superdex 75 10/300 column (Cytiva) in 50 mM Tris, pH 7.5, 150 mM NaCl. MmpS5 was concentrated to 5 mg/ ml for crystallization trials.

Structure determination of Mth MmpS5

Crystallization trials for Mtb and Mth MmpS5 were performed at room temperature using numerous sparse matrix crystallization screens. While Mtb MmpS5 did not produce X-ray diffracting crystals, Mth MmpS5 gave its best crystal hit in PACT 63: 0.2 M sodium iodide, 0.1 M *bis*-Tris propane, pH 6.5, 20% polyethylene glycol (PEG) 3350. The Mth MmpS5 crystal hit was optimized to

Table 1. Data collection and refinement statistics for the Mth MmpS5 crystal structure.

	Mth MmpS5
Data collection	
Space group	$P2_1$
Cell dimensions	
a, *b*, *c* (Å)	50.3, 85.3, 89.1
α, β, γ (°)	90.0, 95.2, 90.0
Resolution (Å)	40.08–1.95 (2.00–1.95)[a]
R_{merge}[b]	0.124 (0.743)
I/σ_I	7.8 (1.8)
Completeness (%)	94.9 (89.9)
Redundancy	4.3 (4.1)
Refinement	
Resolution (Å)	40.08–1.95 (1.97–1.95)
Number of reflections	51 705 (4953)
R_{work}/R_{free}[c]	0.161 (0.239)/0.194 (0.289)
Ramachandran favored (%)	97.4
Ramachandran outliers (%)	0
Number of atoms	4986
Protein	4214
Ligands	226
Water	546
B-factors	24.0
Protein	21.1
Ligands	45.8
Water	37.3
Root-mean-square deviations	
Bond lengths (Å)	0.009
Bond angles (°)	1.05

[a]Values within parentheses refer to the highest shell.
[b]$R_{merge} = \Sigma\Sigma|I_{hkl} - I_{hkl}(j)|/\Sigma I_{hkl}$, where $I_{hkl}(j)$ is the observed intensity and I_{hkl} is the final average value of intensity.
[c]$R_{work} = \Sigma||F_{obs}| - |F_{calc}||/\Sigma|F_{obs}|$ and $R_{free} = \Sigma||F_{obs}| - |F_{calc}||/\Sigma|F_{obs}|$, where all reflections belong to a test set of 10% data randomly selected in Phenix.

0.2 M sodium iodide, 0.1 M Bis-Tris, pH 6.5, 25% PEG 3350. Mth MmpS5 crystals were cryo-cooled in mother liquor supplemented with 20% glycerol, and an iodide-single-wavelength anomalous diffraction dataset was collected at SSRL 12-2 at 8041.5 eV (Table 1). The resulting diffraction data were processed in XDS to 1.95 Å resolution,[30] and the structure was solved in autosol following the placement of eight iodide atoms.[31] Refinement was carried out in phenix.refine[32] and coot[33] to a final R_{work}/R_{free} of 16.1/19.4%.

Size exclusion chromatography to determine the oligomeric state of Mtb and Mth MmpS5

Mtb and Mth MmpS5 purified as described above were run over a Superdex 75 10/300 column (Cytiva) in 50 mM Tris, pH 7.5, 150 mM NaCl. Mtb MmpS5 was applied to the column at concentrations ranging from 0.06 to 0.4 mM, while Mth MmpS5 was applied to the column at concentrations ranging from 0.08 to 0.9 mM. Sizing runs gave two peaks, one for contaminant GST and another for MmpS5. The volume for the MmpS5 eluate peak was plotted as $K_{ave} = (V_{elution} - V_{column})/(V_{column} - V_{void})$ against a set of known standards in order to determine the molecular weight of the oligomeric state in solution.

Liquid chromatography–mass spectrometry to confirm presence of disulfide linkages in Mth MmpS5 and Msm MmpS4/5

E. coli expressed and purified Mth MmpS5 (expression and purification described above) was assayed for the presence of disulfide bonds. Purified Mth MmpS5 was treated with or without (negative control) 0.5 mg/ ml DTT in 50 mM ammonium bicarbonate buffer for 30 min at 80°C. After reduction, 0.5 mg/ ml iodoacetamide (IAA) was added to the samples for 1 h. The IAA-treated proteins were analyzed by MS using liquid chromatography–mass spectrometry (LC–MS) [ACQUITY UPLC (Ultra-Performance Liquid Chromatography) H-class system, Xevo G2-XS QTOF (Quadrupole Time-of-Flight), Waters]. To remove buffer salts, samples were run over a phenyl guard column at 45°C (Acquity UPLC BEH Phenyl VanGuard Pre-column, 130 A˚, 1.7 µm, 2.1 mm × 5 mm, Waters) utilizing a 5-min gradient of 0.1% formic acid into acetonitrile. The Xevo Z-spray source was run in positive ion mode with a capillary voltage of 300 V, and a cone voltage of 40 V (NaCsI calibration, Leu-enkephalin lock-mass), 400–4000 Da. Nitrogen was used as the desolvation gas at 350°C and a flow rate of 800 l/h. Total average mass spectra were reconstructed from the charge state ion series using the MaxEnt1 algorithm from Waters MassLynx software V4.1 SCN949 according to the manufacturer's instructions. To obtain the ion series described, the major peak of the chromatogram was selected for integration before further analysis.

Msm *mmpS4* (MSMEG_0380) and Msm *mmpS5* (MSMEG_0226) genes were assembled into an HygR mycobacterial expression plasmid encoding a C-terminal FLAG-tag using the NEBuilder HIFI DNA assembly (New England Biolabs). Msm expression vectors were electroporated into *M. smegmatis* strain mc^2155, and the transformants were streaked and grown for three days at 37°C on Middlebrook 7H10 agar plates supplemented with 0.2% glycerol, 10% albumin/dextrose/catalase (ADC), and 50 µg/ ml hygromycin. Individual clones were then inoculated into Middlebrook 7H9 media supplemented with 0.2% glycerol, 10% ADS, and 0.05% Tween 80 and grown for 2 days at 37°C. The cells were harvested by centrifugation (5000 r.p.m. for 20 min) and washed twice with Tris-buffered saline (TBS). Pelleted cells were resuspended in iron-free 7H9 media supplemented as described above and grown at 37°C to deplete intracellular iron levels. After 2 days, the culture media were supplemented with 20 µM ferric ammonium citrate. After two more days of growth at 37°C, the cells were harvested by centrifugation (5000 r.p.m., 25 min).

The resulting cell pellets were resuspended and lysed by sonication in buffer (50 mM Tris pH 7.4, 350 mM NaCl, and 10% glycerol). Resuspended cells were incubated for 2 h at 4°C with 1% w/v N-dodecyl-β-D-maltoside. Cellular debris was separated by centrifugation (14 000 r.p.m., 30 min), and the resulting lysates were syringe filtered. Following an overnight incubation at 4°C with Anti-FLAG M2 affinity gel (Sigma–Aldrich), the lysates were centrifuged for 1 min at 2500 r.p.m. and washed three times with TBS buffer. FLAG-tagged MmpS4 or MmpS5 were eluted from the resin with FLAG-peptide (Sigma–Aldrich) and incubated for 30 min at 4°C before centrifuging for 1 min at 2500 r.p.m. and collecting the supernatant containing the purified protein samples. The presence of disulfide bonds in Msm FLAG-tagged MmpS4 and MmpS5 were assayed as described above.

Results and discussion

While the NMR structure of mature Mtb MmpS4 (residues 51–140) was previously determined,[8] the structure of Mtb MmpS5 has not been characterized. As both Mtb MmpS4 and MmpS5 are involved in iron acquisition and are required for virulence, the structures of both proteins are important in understanding their cellular role and their interactions with protein partners and ligands. A sequence comparison of MmpS4 and MmpS5 from various mycobacterium species, including Mtb, Msm, and thermostable Mth, reveals a high level of conservation across

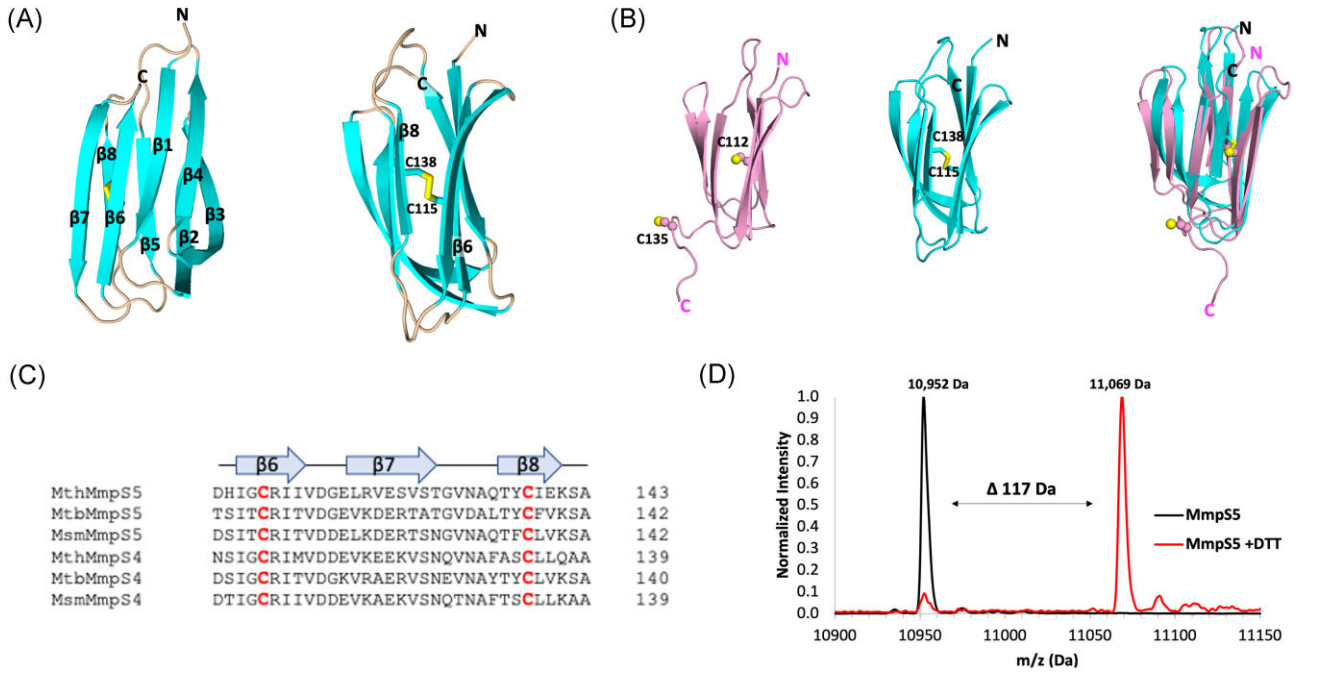

Fig. 1 Mycobacterial MmpS4/S5 proteins have a conserved disulfide bond. (A) Structure of Mth MmpS5 (cyan β-sheets, wheat loops) is shown in a cartoon representation with the conserved disulfide bonds shown as sticks. Secondary structure elements are labeled. (B) Structural comparison of NMR structure of Mtb MmpS4 (pink) with Mth MmpS5 (cyan). Disulfide-bond-forming cysteine residues for Mth MmpS5 are shown as sticks (C115 and C138), while free cysteine residues (C112 and C135) in Mtb MmpS4 are shown as spheres. (C) Sequence alignment of Mtb, Mth, and *M. smegmatis* (Msm) MmpS4 and MmpS5 reveals the conservation of Mth MmpS5 cysteine residues, C115 and C138. Above the sequence is a graphical cartoon of the positions of β6-, β7-, and β8-strands for Mth MmpS5. Msm MmpS4 and MmpS5 are MSMEG_0380 and MSMEG_0226, respectively. (D) Mass spectrometry of intact Mth MmpS5 (untreated with protease) subjected to iodacetamide (IAA) before (black) or dithiothreitol (DTT) after (red). The non-DTT-treated sample mass (10 952 Da) matches the theoretical mass of 10 953 Da (with a disulfide bond). The DTT-treated sample exceeds the theoretical mass by 117 Da, which indicates two IAA modifications (58 Da each, 116 Da total).

organisms (Supplementary Fig. 1). Due to the high degree of sequence similarity (62%, Supplementary Fig. 1) and the fact that sometimes thermostable proteins are more amenable to crystallization,[34,35] we attempted to crystallize both Mtb and Mth MmpS5 proteins. MmpS5 crystallization trials were carried out with the mature forms of Mtb MmpS5 (residues 46–142) and Mth MmpS5 (residues 46–143). While crystal screens for both Mtb and Mth MmpS5 produced initial crystal hits, only Mth MmpS5 yielded diffraction-quality crystals.

Mth MmpS5 crystallized with six subunits in the asymmetric unit, which align with a root-mean-square deviation (rmsd) of 0.29 Å across all residues. Each subunit is characterized by an immunoglobulin-like fold, possessing eight antiparallel β-strands arranged in two β-sheets (β4, β1, β6, β7; β3, β2, β5, and β8) with a Greek key topology (Fig. 1A). Notably, β6 and β8 are covalently attached via a disulfide bond between C115 and C138 that forms across the two β-sheets and tethers them together.

As mentioned above, the structure of an Mth MmpS5 homolog, Mtb MmpS4, was previously determined by NMR.[8] While the Mtb MmpS4 structure aligns well to the Mth MmpS5 structure with an average rmsd of 2.8 Å over 82 of 97 residues (Fig. 1B), the remaining C-terminal portion of the Mtb MmpS4 structure is markedly different from the Mth MmpS5 structure. In the NMR structure, we observe a seven stranded β-sandwich, where the structured β8 observed in the Mth MmpS5 is instead a highly mobile random coil in Mtb MmpS4 and does not participate in the Mtb MmpS4 β-sheet (Fig. 1B). Notably, the Mth MmpS5 cysteine residues (C115 and C138), which covalently link β6 and β8 in the crystal structure, are conserved in both Mtb MmpS4 (C112 and C135) and Mtb MmpS5, as well as the Msm homologs (Fig. 1C, Supplementary Fig. 1). No disulfide bond is observed in the Mtb MmpS4 structure.[8] Moreover, Mtb MmpS4 C112 and Mth MmpS5 C115, situated in β6, align when the two structures are superimposed (Fig. 1B). As the NMR experiments were performed in the presence of 1 mM DTT, it is likely that Mtb MmpS4 possesses a disulfide bond under non-reduced conditions, which is not captured in the structure due to presence of reductant.

To ensure that the disulfide bond observed in the X-ray structure of Mth MmpS5 was not a product of crystallization, we utilized MS to confirm that Mth MmpS5 has a disulfide bond in solution. Non-reduced and reduced (in the presence of DTT) Mth MmpS5 samples were treated with IAA, and the resulting molecular weights were determined by MS. When IAA covalently modifies free protonated cysteine, the mass shift is 57 Da per cysteine residue, and as Mth MmpS5 has two cysteines, we expect a total shift of 114 Da. Non-reduced Mth MmpS5 has a mass of 10 952 Da, which is comparable to the theoretical mass for Mth MmpS5 of 10 953 Da (parent mass minus two protons lost due to the putative disulfide bond), suggesting that the two cysteines are forming a disulfide bond and are not available for IAA modification (Fig. 1D). In the reduced sample, the dominant peak gives a mass of 11 069 Da, which is a +117 Da mass shift from the observed non-reduced mass (Fig. 1D). This represents a sample that has had its disulfide bond reduced and modified by two molecules of IAA (expected mass shift of 116 Da). As IAA modification of the Mth MmpS5 cysteine residues is only observed under reducing conditions, this suggests that under native (non-reduced) conditions in solution the two Mth MmpS5 cysteine residues form a disulfide bond, thus suggesting that the observed Mth MmpS5 disulfide bond in the structure is not a crystallographic artifact.

To verify the *in vivo* relevance of the MmpS5 disulfide bond, Msm MmpS4 and MmpS5 with C-terminal FLAG tags were expressed in Msm and purified for analysis by MS. Msm MmpS4 and MmpS5 were analyzed before and after reduction by DTT followed by IAA treatment, as described above for Mth MmpS5. Non-reduced IAA-treated Msm MmpS4 and Msm MmpS5 have masses of 17 979 and 18 110 Da, respectively (Supplementary Fig. 2). However, reduced IAA-treated Msm MmpS4 and MmpS5 have masses of 18 094 and 18 225 Da, respectively. The resulting molecular weight shifts after the reduction of 115 Da for both proteins are consistent with the modification of two cysteine residues by IAA, confirming that *in vivo* native (non-reduced) Msm MmpS4 and MmpS5 proteins each has a biologically relevant disulfide bond.

Mth MmpS5 forms two different potential dimers in the asymmetric unit (Supplementary Fig. 3). The first potential dimer (Dimer 1) is formed between subunits A/C and D/F with a dimerization interface comprising ∼10% of the protein surface area (Supplementary Fig. 3A). Moreover, 11 hydrogen bonds and 12 hydrogen bonds are formed at the A/C and D/F interface, respectively. Dimer 1 interface interactions are primarily between backbone atoms on $\beta 7$ of each subunit and symmetrical interactions occur between $\beta 7$ and $\beta 8$ sidechains from each subunit, essentially forming extended β-sheets between the two subunits (Supplementary Fig. 3A). Symmetrical backbone hydrogen bonds include residues E126, S127, V128, S129, and T130, and two symmetrical sets of sidechain hydrogen bonds involve S127 and S129′ and Q135 and Y137′ across subunits (Supplementary Fig. 3A). The dimer interface results in a curvature of ∼75–80° between the two planar β-sheet subunits (Supplementary Fig. 4A). Another interesting facet of Dimer 1 is that at the curved dimeric interface there are several glycerol and PEG molecules, and these small ligands are at a higher density near the final β-strand, specifically near Y137 and K141 (Supplementary Fig. 4B). Another potential dimer (Dimer 2) in the asymmetric unit involves A/B, D/E, and C/F subunit pairs (Supplementary Fig. 4B). This dimerization interface comprises ∼15% of the surface area of each subunit with five hydrogen bonds between the sidechains from residues on $\beta 1$ and $\beta 4$ from each subunit. As Dimer 1 involves substantially more interactions at the dimerization interface, we believe Dimer 1 is more likely to be physiologically relevant.

As Mth MmpS5 forms dimers in the asymmetric unit, we performed size exclusion chromatography to determine the oligomeric state of Mth MmpS5 and Mtb MmpS5 in solution. Strikingly, both Mth MmpS5 and Mtb MmpS5 elute from a sizing column at a volume that corresponds to a dimer in solution (Fig. 2C and Supplementary Fig. 5). Notably, elution volumes did not change despite testing a range of protein concentrations (0.06–0.9 mM, data not shown). From the elution volume, Mth and Mtb MmpS5 elute at a molecular weight of ∼22 kDa, which infers both Mth and Mtb MmpS5 are dimers in solution. As the Mth Dimer 1 interface has backbone interactions between $\beta 7$ strands, it is likely that these interactions would persist in Mtb, however, while Y137 is conserved between Mtb and Mth, the $\beta 7/\beta 8$-strand side chain interactions are likely to vary as S127, S129, and Q135 are not conserved (Supplementary Fig. 1). Notably, the NMR structure of Mtb MmpS4 is monomeric.[8] However, as the NMR structure lacks a structured $\beta 8$-strand, the surface required for the formation of Dimer 1 would be incomplete, preventing dimerization. Dimer 2, however, would not have been disturbed in the absence of a structured $\beta 8$-strand, and further suggests that Dimer 1 is likely the relevant oligomeric state.

Structural homologs of MmpS5 were found using a Dali search (Supplementary Table 1A).[36] Most of the identified structural homologs are not well characterized, although one eukaryotic and two bacterial proteins are of particular interest due to similar dimerization interfaces and the presence of a bound ligand or protein partner. These structural homologs, the SoxYZ heterodimer,[37–39] human TMED1,[40] and the *E. coli* K12 F18 fimbriae adhesin FedF[41] align to Mth MmpS5 with 3–4.6 Å rmsd over 64–72 residues (Supplementary Fig. 6). SoxYZ is a heterodimeric complex that binds sulfur adducts and transfers them between enzymes in the sulfur-oxidizing (Sox) multi-enzyme system.[37,39] TMED1 belongs to a transmembrane sorting receptor family in the endoplasmic reticulum and Golgi and is a central regulator for biomolecule secretion.[40] F18 fimbriae attach to glycosphingolipids associated with specific blood types via FedF, which binds the ABH type 1 blood group glycan.[41] Like Mth MmpS5, both TMED1 (Supplementary Fig. 6C) and FedF possess disulfide bonds (Supplementary Fig. 6D). While the disulfide bond locations do not align well to each other or to Mth MmpS5, their presence in these structural homologs is intriguing.

Both the SoxYZ heterodimer and TMED1 dimer align closely to Mth MmpS5 Dimer 1 (Fig. 2). SoxY and SoxZ form a heterodimer in the Sox system, where SoxY and SoxZ differ in that SoxY has an N-terminal accessory helix, and SoxZ contains an extended Z-loop.[37–39] In the SoxYZ heterodimer, SoxY has the catalytic cysteine that carries intermediates between enzymes. One of the enzymes that SoxYZ interacts with is SoxB (Fig. 2Aii).[37–39] While Mth MmpS5 aligns to both SoxY and SoxZ subunits, it aligns more closely to SoxZ (Supplementary Fig. 6A and B, Supplementary Tables 1A and B). Interestingly, the SoxYZ heterodimer and the MmpS5 Dimer 1 align closely, where both dimers superimpose and share a concave face. Notably, the SoxYZ concave surface faces SoxB, suggesting that the concave face of MmpS5 could be important for protein–protein interactions (Fig. 2A). This similarity between dimers is also observed for the TMED1 dimer and Mth MmpS5 Dimer 1 (Fig. 2B). In solution, TMED1 is a dimer where conserved residues Q49 and Y52 contribute to the oligomerization interface. Interestingly, TMED1 Q49 and Y52 superimpose with MmpS5 Q135 and Y137 (Fig. 2B), which, as described above, are hydrogen bonding residues at the Dimer 1 interface. As both the SoxYZ heterodimer and TMED1 dimer align closely to Mth MmpS5 Dimer 1, these structures suggest that Dimer 1 could have physiological relevance.

Many ligands from the crystallization solution were detected in the Mth MmpS5 structure. While these ligands are not physiologically relevant, their binding locations could represent the location of physiological ligand binding sites or protein interaction surfaces. When all the Mth MmpS5 subunits are superimposed, a few locations with high ligand colocalization are apparent (Fig. 3A and Supplementary Fig. 4B). Specifically, several PEG and glycerol molecules overlay and are coordinated by K141. This ligand-binding site is also marked by interactions with Y137 and is close to H103. Another binding site for several glycerol molecules is coordinated by D69, N71, R81, Q107, and Q135. Strikingly, the opposite face of the MmpS5 β-sheet does not coordinate any crystallization ligands. Thus, MmpS5 appears to have a more charged, interaction-rich face, and a less charged, non-interactive face.

Interestingly, the superimposition of Mth MmpS5 with SoxY in the SoxYZ heterodimer places this ligand-binding site at the SoxY/SoxB interface—providing support to the possibility that the ligand-trapping face of MmpS5 could be important for protein–protein interactions (Fig. 3B). Notably, the charged MmpS5 face aligns to the ligand binding face of its structural homolog, FedF (Supplementary Figs. 6D and S7). FedF also forms a dimer, which is less planar than MmpS5 Dimer 1 and was crystallized with a blood

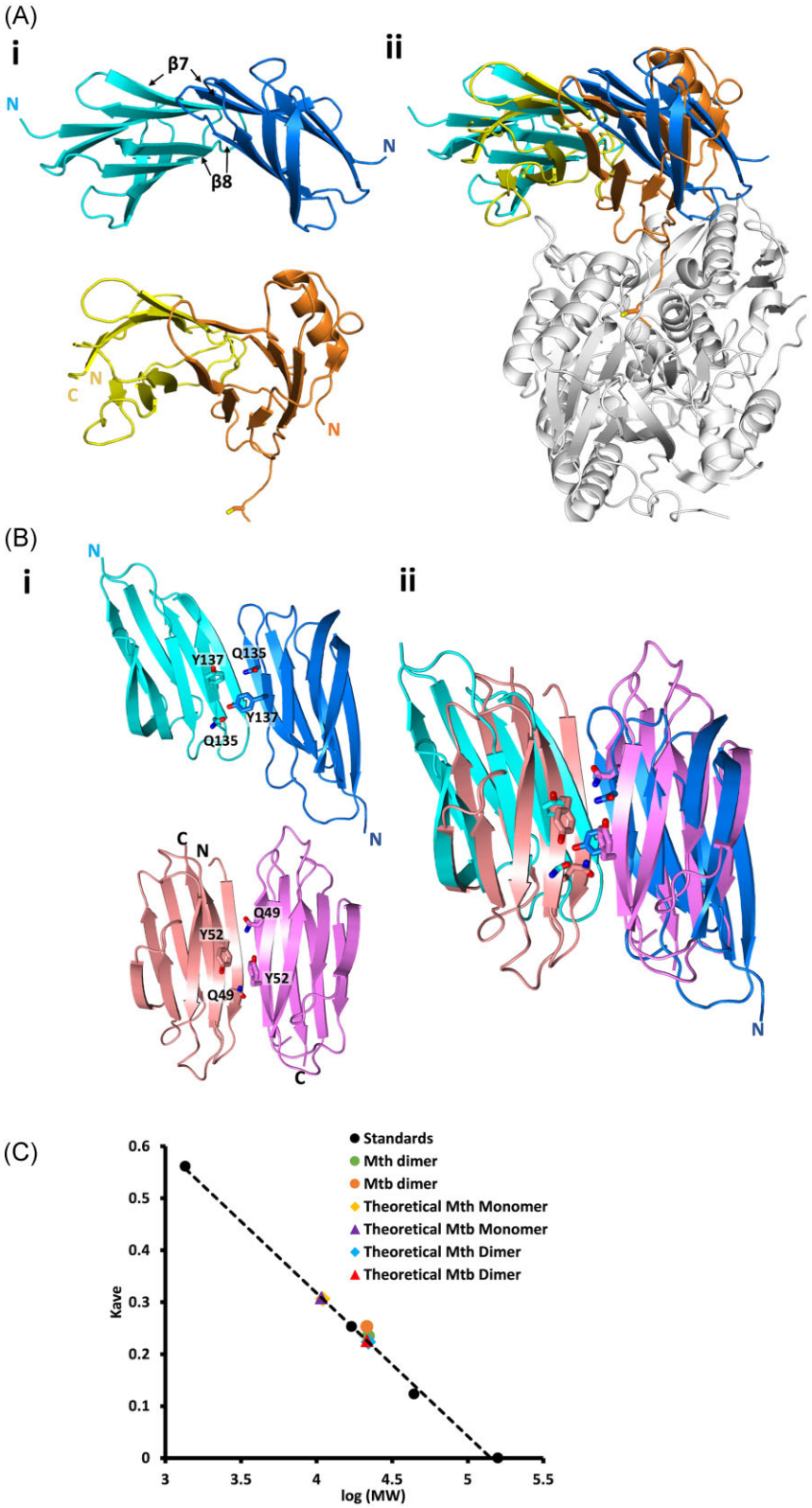

Fig. 2 Mth MmpS5 forms a dimer in solution, and Dimer 1 has structural similarities to the SoxYZ heterodimer and TMED1 homodimer. Mth MmpS5 Dimer 1 subunits are colored in cyan and marine blue. (A) Comparison of Mth MmpS5 Dimer 1 with SoxYZ heterodimer. (i) Direct comparison of Dimer 1 with SoxYZ dimer (SoxY and SoxZ colored in orange and yellow, respectively). (ii) Superimposition of the dimers in context of the complex with SoxB (white cartoon). (B) Comparison of Mth MmpS5 Dimer 1 and TMED1 homodimer (colored in salmon and pink). (i) Direct comparison of homodimers shows conservation of residues at the dimerization interface: Mth MmpS5 Q135 and Y137 with TMED1 Q49 and Y52. Residues shown as sticks. (ii) Overlay of the homodimers highlights similarities between the two dimers. (C) Size exclusion chromatography with Mth MmpS5 and Mtb MmpS5 revealed that both MmpS5 proteins are dimeric in solution. A linear plot of the K_{ave} vs log (molecular weight) for protein standards was used to extrapolate the molecular weights of the MmpS5 protein oligomers. Here, the K_{ave} for Mth MmpS5 (0.2 mM) and Mtb MmpS5 (0.2 mM) is plotted against the theoretical mass of their monomers (~11 kDa) and homodimers (~22 kDa) in the context of the standards. Results suggest they are both dimeric in solution.

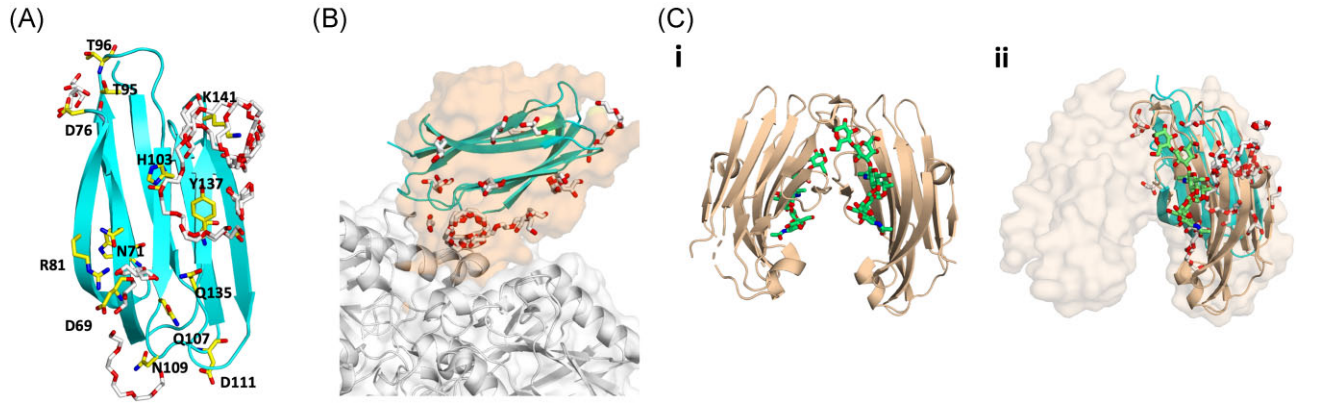

Fig. 3 Mth MmpS5 has crystallographic ligand-binding surfaces in similar locations to ligand binding and protein binding surfaces in structural homologs: SoxYZ and FedF. (A) Alignment of the six Mth MmpS5 subunits (represented by a cyan cartoon) in the asymmetric unit shows colocalization of bound crystallographic ligands near H103, Y137, and K141. Ligand-coordinating residues are shown as yellow sticks, ligands are shown as white sticks. (B) Alignment of Mth MmpS5 to SoxY in the context of the SoxYZ/SoxB complex shows that the Mth MmpS5 crystallographic ligand binding occurs at the SoxY/SoxB interface. SoxY and SoxB are colored in orange and white, respectively. SoxY is represented as a semi-transparent molecular surface (orange) with the cartoon omitted for clarity. Ligands colored as in (A). (C) FedF (colored in wheat) was crystallized with blood group A type 1 hexaglycosylceramide (i), the FedF dimer is in cartoon representation with one sugar bound per subunit (shown in green sticks). When Mth MmpS5 is aligned to one FedF subunit (ii), the Mth MmpS5 crystallographic ligands bind near the FedF sugar binding side. Here, the FedF dimer is represented by the semi-transparent molecular surface.

group A type 1 hexa-saccharide bound[41] (Fig. 3C). The FedF sheet curves towards its ligand-binding site (Fig. 3Ci), which involves a few key residues on one surface of the β-sheet: Q47, Y49, and H88. These β-sheet surface residues roughly align to Mth MmpS5 residues Q135, Y137, and H103 (Fig. 3A) on the proposed interaction face of MmpS5.

Results from the Mth MmpS5 structural homologs provide further insights into MmpS5. First, the Mth MmpS5 Dimer 1 may be biologically important as both the SoxYZ heterodimer and TMED1 dimer align closely to Mth MmpS5 Dimer 1. Second, Mth MmpS5 residues Q135 and Y137 align to TMED1 and FedF residues that are either at the dimer interface or involved in ligand interactions, respectively, indicating that these residues could be important for ligand binding or protein interactions in Mth MmpS5. When comparing Mth MmpS5 to the Mtb paralogs, we found that Mth Q135 is not conserved in Mtb MmpS4/5, whereas Y137 is conserved and also proximal to the disulfide-bond-forming cysteine residue, C138 (Supplementary Fig. 1). Y137 is conserved across MmpS homologs, suggesting that it is a great candidate for protein–protein interactions or ligand binding.

Conclusion

Herein, we demonstrate that the structure of MmpS5 is an immunoglobulin-like fold comprising two four-stranded antiparallel β-sheets with one disulfide bond (C115 and C138) linking β6 and β8 and tethering the two β-sheets. As the disulfide bond was absent from the NMR structure of Mtb MmpS5, we did MS analysis on Mth MmpS5 expressed in *E. coli* and Msm MmpS4 and MmpS5 expressed in *M. smegmatis* and confirmed the presence of the disulfide bond in both environments. These analyses, supplemented by sequence analysis of MmpS4 and MmpS5 from a variety of mycobacterial species, indicate that the disulfide bond is likely a common feature in MmpS4 and MmpS5. Several structural homologs of Mth MmpS5 also have disulfide bonds (Supplementary Fig. 6C and D), and while the location is not consistent, it is interesting to note that disulfide bonds are a common occurrence in this protein family and that they may have a role in maintaining a specific conformation required for protein function or stability. It should be noted that the importance and physiological role of the disulfide bond in MmpS4 and MmpS5 still require elucidation.

The crystal structure and size exclusion chromatography show that Mth MmpS5 can form a dimer in solution. While the Mtb MmpS4 NMR structure is monomeric, the dimeric interface of Mth MmpS5 Dimer 1 involves the disulfide-bonded β8-strand (Fig. 2B), which is absent from the MmpS4 NMR structure (Fig. 1B). We believe that the dimeric structure could be a common feature in MmpS4 and MmpS5, and that Mtb MmpS4 in non-reducing conditions would also dimerize.

MmpS4 and MmpS5 proteins are involved in siderophore and anti-TB drug efflux as accessory proteins to MmpL4 and MmpL5, respectively. To better understand the role of the MmpS4/L4 or MmpS5/L5 complexes in Mtb, two papers have performed modeling to characterize the interaction of MmpS5 and MmpL5.[42,43] Notably, these simulation attempts were based on the NMR structure of reduced Mtb MmpS4. The occurrence of the disulfide bond in the MmpS4 structure dramatically changes the overall shape and molecular surface electrostatics of the protein (Supplementary Fig. 7), suggesting that utilizing a non-reduced MmpS5 structure in simulation and docking studies is imperative. Lastly, the Mth MmpS5 crystal structure highlights residues that are likely to be involved in protein–protein or protein– ligand interactions such as Y137 and K141. In summary, understanding the structure and oligomeric state of MmpS4 and MmpS5 is critical to empowering modeling efforts, and the structural insights revealed in this paper will greatly assist future simulation experiments.

Supplementary material

Supplementary data are available at *Metallomics* online.

Acknowledgments

We thank the Advanced Light Source at Berkeley National Laboratories (ALS) and the Stanford Synchrotron Radiation Lightsource (SSRL) for their invaluable help in data collection.

Funding

C.W.G. (UCI) and C.S. (UMass) thank the National Institutes of Health (NIH) for financial support through P01-AI095208. Additionally, R.M. (UCI) thanks the NIH for support from a predoctoral training grant [T32 AI141346].

Conflicts of interest

The authors declare no conflicts of interest.

Data availability

The structural data (coordinates and structure factors) underlying this article are available in the Protein Data Bank at https://www.rcsb.org/ and can be accessed with the PDB ID 8EM5. The remaining data underlying this article will be shared on reasonable request to the corresponding author.

References

1. World Health Organization. *Global Tuberculosis Report 2022*. https://www.who.int/teams/global-tuberculosis-programme/tb-reports/global-tuberculosis-report-2022 (6 October 2022, date last accessed).
2. B. Rojano, J. A. Caminero and M. Hayek, Curving tuberculosis: current trends and future needs, *Ann. Glob. Health*, 2019, 85(1), 5. https://doi.org/10.5334/aogh.2415
3. C. M. Gill, L. Dolan, L. M. Piggott and A. M. McLaughlin, New developments in tuberculosis diagnosis and treatment, *Breathe (Sheff)*, 2022, 18(1), 210149. https://doi.org/10.1183/20734735.0149-2021
4. K. Sharma, F. Ahmed, T. Sharma, A. Grover, M. Agarwal and S. Grover, Potential repurposed drug candidates for tuberculosis treatment: progress and update of drugs identified in over a decade, *ACS Omega*, 2023, 8(20), 17362–17380. https://doi.org/10.1021/acsomega.2c05511
5. A. Chao, P. J. Sieminski, C. P. Owens and C. W. Goulding, Iron acquisition in *Mycobacterium tuberculosis*, *Chem. Rev.*, 2019, 119(2), 1193–1220. https://doi.org/10.1021/acs.chemrev.8b00285
6. C. M. Jones, R. M. Wells, A. V. Madduri, M. B. Renfrow, C. Ratledge, D. B. Moody and M. Niederweis, Self-poisoning of *Mycobacterium tuberculosis* by interrupting siderophore recycling, *Proc. Natl. Acad. Sci. USA*, 2014, 111(5), 1945–1950. [pii] https://doi.org/10.1073/pnas.1311402111
7. C. Ratledge, Iron, mycobacteria and tuberculosis, *Tuberculosis (Edinb.)*, 2004, 84(1–2),110–130 https://doi.org/10.1016/j.tube.2003.08.012
8. R. M. Wells, C. M. Jones, Z. Xi, A. Speer, O. Danilchanka, K. S. Doornbos, P. Sun, F. Wu, C. Tian and M. Niederweis, Discovery of a siderophore export system essential for virulence of *Mycobacterium tuberculosis*, *PLoS Pathog.*, 2013, 9(1), e1003120. https://doi.org/10.1371/journal.ppat.1003120
9. P. Domenech, M. B. Reed and C. E. Barry, 3rd, Contribution of the *Mycobacterium tuberculosis* MmpL protein family to virulence and drug resistance, *Infect. Immun.*, 2005, 73(6), 3492–3501. https://doi.org/10.1128/IAI.73.6.3492-3501.2005.
10. C. Chalut, MmpL transporter-mediated export of cell-wall associated lipids and siderophores in mycobacteria, *Tuberculosis (Edinb.)*, 2016, 100:32–45. https://doi.org/10.1016/j.tube.2016.06.004
11. A. Viljoen, V. Dubois, F. Girard-Misguich, M. Blaise, J. L. Herrmann and L. Kremer, The diverse family of MmpL transporters in mycobacteria: from regulation to antimicrobial developments, *Mol. Microbiol.*, 2017, 104(6), 889–904. https://doi.org/10.1111/mmi.13675
12. J. Briffotaux, W. Huang, X. Wang and B. Gicquel, MmpS5/MmpL5 as an efflux pump in Mycobacterium species, *Tuberculosis (Edinb.)*, 2017, 107, 13–19. https://doi.org/10.1016/j.tube.2017.08.001
13. N. Chim, R. Torres, Y. Liu, J. Capri, G. Batot, J. P. Whitelegge and C. W. Goulding, The structure and interactions of periplasmic domains of crucial MmpL membrane proteins from mycobacterium tuberculosis, *Chem. Biol.*, 2015, 22(8), 1098–1107. https://doi.org/10.1016/j.chembiol.2015.07.013
14. B. Zhang, J. Li, X. Yang, L. Wu, J. Zhang, Y. Yang, Y. Zhao, L. Zhang, X. Yang, X. Yang, X. Cheng, Z. Liu, B. Jiang, H. Jiang, L. W. Guddat, H. Yang and Z. Rao, Crystal structures of membrane transporter MmpL3, an anti-TB drug target, *Cell*, 2019, 176(3), 636–648 e13. https://doi.org/10.1016/j.cell.2019.01.003
15. H. I. Zgurskaya, G. Malloci, B. Chandar, A. V. Vargiu and P. Ruggerone, Bacterial efflux transporters' polyspecificity—a gift and a curse?, *Curr. Opin. Microbiol.*, 2021, 61, 115–123. https://doi.org/10.1016/j.mib.2021.03.009
16. O. Adams, J. C. Deme, J. L. Parker, C. R. Consortium, P. W. Fowler, S. M. Lea and S. Newstead, Cryo-EM structure and resistance landscape of M. tuberculosis MmpL3: an emergent therapeutic target, *Structure*, 2021, 29(10), 1182–1191 e4. https://doi.org/10.1016/j.str.2021.06.013
17. C. C. Su, P. A. Klenotic, J. R. Bolla, G. E. Purdy, C. V. Robinson and E. W. Yu, MmpL3 is a lipid transporter that binds trehalose monomycolate and phosphatidylethanolamine, *Proc. Natl. Acad. Sci. USA*, 2019, 116(23), 11241–11246. https://doi.org/10.1073/pnas.1901346116
18. K. Yamamoto, N. Nakata, T. Mukai, I. Kawagishi and M. Ato, Co-expression of MmpS5 and MmpL5 contributes to both efflux transporter MmpL5 trimerization and drug resistance in mycobacterium tuberculosis, *mSphere*, 2021, 6(1), e00518–e00520. https://doi.org/10.1128/mSphere.00518-20
19. L. Zhang, R. C. Hendrickson, V. Meikle, E. J. Lefkowitz, T. R. Ioerger and M. Niederweis, Comprehensive analysis of iron utilization by mycobacterium tuberculosis, *PLoS Pathog.*, 2020, 16(2), e1008337. https://doi.org/10.1371/journal.ppat.1008337
20. G. Lamichhane, S. Tyagi and W. R. Bishai, Designer arrays for defined mutant analysis to detect genes essential for survival of mycobacterium tuberculosis in mouse lungs, *Infect. Immun.*, 2005, 73(4), 2533–2540. https://doi.org/10.1128/IAI.73.4.2533-2540.2005
21. D. C. Alexander, R. Vasireddy, S. Vasireddy, J. V. Philley, B. A. Brown-Elliott, B. J. Perry, D. E. Griffith, J. L. Benwill, A. D. Cameron and R. J. Wallace, Jr, Emergence of mmpT5 variants during Bedaquiline treatment of mycobacterium intracellulare Lung disease, *J. Clin. Microbiol.*, 2017, 55(2), 574–584. https://doi.org/10.1128/JCM.02087-16
22. K. Andries, C. Villellas, N. Coeck, K. Thys, T. Gevers, L. Vranckx, N. Lounis, B. C. de Jong and A. Koul, Acquired resistance of mycobacterium tuberculosis to bedaquiline, *PLoS One*, 2014, 9(7), e102135. https://doi.org/10.1371/journal.pone.0102135
23. Q. Guo, J. Bi, Q. Lin, T. Ye, Z. Wang, Z. Wang, L. Liu and G. Zhang, Whole genome sequencing identifies novel mutations associated with Bedaquiline resistance in mycobacterium tuberculosis, *Front. Cell. Infect. Microbiol.*, 2022, 12, 807095. https://doi.org/10.3389/fcimb.2022.807095
24. I. Halloum, A. Viljoen, V. Khanna, D. Craig, C. Bouchier, R. Brosch, G. Coxon and L. Kremer, Resistance to thiacetazone derivatives active against mycobacterium abscessus involves mutations in the MmpL5 transcriptional repressor MAB_4384, *Antimicrob.*

Agents Chemother., 2017, 61(4), e02509–e02516. https://doi.org/10.1128/AAC.02509-16
25. R. C. Hartkoorn, S. Uplekar and S. T. Cole, Cross-resistance between clofazimine and bedaquiline through upregulation of MmpL5 in *Mycobacterium tuberculosis*, *Antimicrob. Agents Chemother.*, 2014, 58(5), 2979–2981. https://doi.org/10.1128/AAC.00037-14
26. A. Milano, M. R. Pasca, R. Provvedi, A. P. Lucarelli, G. Manina, A. L. Ribeiro, R. Manganelli and G. Riccardi, Azole resistance in *Mycobacterium tuberculosis* is mediated by the MmpS5-MmpL5 efflux system, *Tuberculosis (Edinb.)*, 2009, 89(1), 84–90. https://doi.org/10.1016/j.tube.2008.08.003
27. C. Villellas, N. Coeck, C. J. Meehan, N. Lounis, B. de Jong, L. Rigouts and K. Andries, Unexpected high prevalence of resistance-associated Rv0678 variants in MDR-TB patients without documented prior use of clofazimine or bedaquiline, *J. Antimicrob. Chemother.*, 2017, 72(3), 684–690. https://doi.org/10.1093/jac/dkw502
28. J. Xu, P. J. Converse, A. M. Upton, K. Mdluli, N. Fotouhi and E. L. Nuermberger, Comparative efficacy of the novel diarylquinoline TBAJ-587 and Bedaquiline against a resistant Rv0678 mutant in a mouse model of tuberculosis, *Antimicrob. Agents Chemother.*, 2021, 65(4), e02418–e02420. https://doi.org/10.1128/AAC.02418-20
29. V. Meikle, L. Zhang and M. Niederweis, Intricate link between siderophore secretion and drug efflux in *Mycobacterium tuberculosis*, *Antimicrob. Agents Chemother.*, 2023, 67(10), 1–20. https://doi.org/10.1128/aac.01629-22
30. W. Kabsch, XDS, *Acta. Crystallogr. Sect. D Biol. Crystallogr.*, 2010, D66, 125–132. https://doi.org/10.1107/S0907444909047337
31. T. C. Terwilliger, P. D. Adams, R. J. Read, A. J. McCoy, N. W. Moriarty, R. W. Grosse-Kunstleve, P. V. Afonine, P. H. Zwart and L. W. Hung, Decision-making in structure solution using bayesian estimates of map quality: the PHENIX AutoSol wizard, *Acta Crystallogr. Sect. D Biol. Crystallogr.*, 2009, 65(6), 582–601. https://doi.org/10.1107/S0907444909012098
32. P. V. Afonine, R. W. Grosse-Kunstleve, N. Echols, J. J. Headd, N. W. Moriarty, M. Mustyakimov, T. C. Terwilliger, A. Urzhumtsev, P. H. Zwart and P. D. Adams, Towards automated crystallographic structure refinement with phenix.refine, *Acta Crystallogr. Sect. D Biol. Crystallogr.*, 2012, 68(4), 352–367. https://doi.org/10.1107/S0907444912001308
33. P. Emsley and K. Cowtan, Coot: model-building tools for molecular graphics, *Acta Crystallogr. Sec. D Biol. Crystallogr.*, 2004, 60(Pt 12 Pt 1), 2126–2132. https://doi.org/10.1107/S0907444904019158
34. R. Scandurra, V. Consalvi, R. Chiaraluce, L. Politi and P. C. Engel, Protein thermostability in extremophiles, *Biochimie*, 1998, 80(11), 933–941. https://doi.org/10.1016/s0300-9084(00)88890-2
35. B. G. Fox, C. Goulding, M. G. Malkowski, L. Stewart and A. Deacon, Structural genomics: from genes to structures with valuable materials and many questions in between, *Nat. Methods*, 2008, 5(2), 129–132. https://doi.org/10.1038/nmeth0208-129
36. L. Holm and P. Rosenstrom, Dali server: conservation mapping in 3D, *Nucleic. Acids. Res.*, 2010, 38(Web Server issue), W545–W549. https://doi.org/10.1093/nar/gkq366
37. D. B. Grabarczyk, P. E. Chappell, S. Johnson, L. S. Stelzl, S. M. Lea and B. C. Berks, Structural basis for specificity and promiscuity in a carrier protein/enzyme system from the sulfur cycle, *Proc. Natl. Acad. Sci. USA*, 2015, 112(52), E7166–E7175. https://doi.org/10.1073/pnas.1506386112
38. V. Sauve, S. Bruno, B. C. Berks and A. M. Hemmings, The SoxYZ complex carries sulfur cycle intermediates on a peptide swinging arm, *J. Biol. Chem.*, 2007, 282(32), 23194–23204. https://doi.org/10.1074/jbc.M701602200
39. J. Stout, G. Van Driessche, S. N. Savvides and J. Van Beeumen, X-ray crystallographic analysis of the sulfur carrier protein SoxY from *Chlorobium limicola f. thiosulfatophilum* reveals a tetrameric structure, *Protein Sci.*, 2007, 16(4), 589–601. https://doi.org/10.1110/ps.062633607
40. D. Mota, I. A. Cardoso, R. M. Mori, M. R. B. Batista, L. G. M. Basso, M. C. Nonato, A. J. Costa-Filho and L. F. S. Mendes, Structural and thermodynamic analyses of human TMED1 (p24γ1) Golgi dynamics, *Biochimie*, 2022, 192, 72–82. https://doi.org/10.1016/j.biochi.2021.10.002
41. K. Moonens, J. Bouckaert, A. Coddens, T. Tran, S. Panjikar, M. De Kerpel, E. Cox, H. Remaut and H. De Greve, Structural insight in histo-blood group binding by the F18 fimbrial adhesin FedF, *Mol. Microbiol.*, 2012, 86(1), 82–95. https://doi.org/10.1111/j.1365-2958.2012.08174.x
42. P. Sandhu and Y. Akhter, Siderophore transport by MmpL5-MmpS5 protein complex in mycobacterium tuberculosis, *J. Inorg. Biochem.*, 2017, 170, 75–84. https://doi.org/10.1016/j.jinorgbio.2017.02.013
43. M. Shahbaaz, D. A. Maslov, A. A. Vatlin, V. N. Danilenko, M. Grishina and A. Christoffels, Repurposing based identification of novel inhibitors against MmpS5-MmpL5 efflux pump of *Mycobacterium smegmatis*: a combined in silico and *in vitro* study, *Biomedicines*, 2022, 10(2), 333. https://doi.org/10.3390/biomedicines10020333

Received: October 31, 2023. **Accepted:** February 10, 2024